ARTICLE

Mechanistic Insights into UV-Induced Electron Transfer from PCBM to Titanium Oxide in Inverted-Type Organic Thin Film Solar Cells Using AC Impedance Spectroscopy

Takayuki Kuwabara,* Chiaki Iwata, Takahiro Yamaguchi, and Kohshin Takahashi*

Graduate School of Natural Science and Technology, Kanazawa University, Kakuma-machi, Kanazawa, Ishikawa 920-1192, Japan

ABSTRACT An inverted organic bulk-heterojunction solar cell containing amorphous titanium oxide (TiOx) as an electron collection electrode with the structure ITO/TiO_x/[6,6]-phenyl C_{61} butyric acid methyl ester (PCBM): regioregular poly(3-hexylthiophene) (P3HT)/poly(3,4-ethylenedioxylenethiophene):poly(4-styrene sulfonic acid)/Au (TiO_x cell) was fabricated. Its complicated photovoltaic properties were investigated by photocurrent−voltage and alternating current impedance spectroscopy measurements. The TiO_x cell required a significant amount of time (approximately 60 min) to reach its maximum power conversion efficiency (PCE) of 2.6%. To investigate the reason for this slow photoresponse, we investigated the influences of UV light and water molecules adsorbed on the TiO_x layer. Surface treatment of the TiO_x cell with water induced a rapid photoresponse and enhanced the performance, giving a PCE of 2.97%. However, the durability of the treated cell was considerably inferior that of the untreated cell because of UV-induced photodegradation. The cause of the rapid photoresponse of the treated cell was attributed to the formation of hydrogen bonds between adsorbed water molecules and carbonyl oxygen atoms in PCBM close to the TiO_x surface. When the TiO_x surface was positively charged by UV-induced holes, the carbonyl oxygen in PCBM close to the TiO_x surface can quickly join to the TiO_x surface, rapidly transporting photogenerated electrons from PCBM to TiO_x in competition with the photocatalyzed degradation. The experimental results suggested that the slow photoresponse of the untreated TiO_x cell was because the morphology of the photoactive organic layer changed gradually upon irradiation to improve the transport of photocarriers at the TiO_x/PCBM:P3HT interface.

KEYWORDS: alternating current impedance spectroscopy • bulk heterojunction • inverted structure • organic thin film solar cells • photocurrent response • titanium oxide

1. INTRODUCTION

Organic solar cells have attracted considerable interest as a candidate for the next generation of solar cells because they provide a low-cost, low-environmental-load, flexible, and lightweight alternative to the silicon solar cells currently in use. Though there are many examples directed at achieving highly efficient organic solar cells, attempts to develop a cell with high durability and large photoactive area are still few. Recently, significant improvement in organic bulk heterojunction solar cells has been achieved by the synthesis of new donor polymers and acceptor fullerene derivatives and optimization of the phase separation between donor and acceptor domains in the active layer, allowing a power conversion efficiency (PCE) of 5−6% to be attained (1−4). However, the behavior of electron or hole transport at interfaces in organic solar cells is not understood sufficiently yet despite it being very important to improve cell performance.

Current−voltage ($I-V$) measurements are commonly employed to evaluate the cell performance and analyze the series and shunt resistances in the cell. The $I-V$ profile provides the photoelectric conversion properties as a whole; however, it is unsuitable for describing localized information such as the electric properties of each layer. Alternating current (ac) impedance spectroscopy (IS) is an electrical measurement technique used to monitor the current response as a function of frequency when an ac voltage is applied. Using ac IS, it is possible to observe bulk and interfacial electrical properties that cannot be observed by a direct current (dc) method, because the speed of the electric response of each component is different on the microscopic time scale. This method has been used to study charge carrier relaxation and transportation in organic devices such as dye-sensitized solar cells (5, 6) and organic light-emitting diodes (7−9), providing mechanistic insights to improve these devices. On the other hand, IS has seldom been used to characterize organic thin-film solar cells because reasonable accuracy was not obtained due to the rapid performance degradation of the cells under light irradiation. Even so, a few researchers have managed to study the electrical properties of solar cells using IS, providing important information about exciton dissociation at the donor/acceptor interface and the mobility and lifetime of charge carriers in the organic active layer (10−12). However, these studies were performed on "normal solar cells", in which

* Corresponding author. Tel: +81-76-234-4770. Fax: +81-76-234-4800. E-mail: tkuwa@t.kanazawa-u.ac.jp.

Received for review April 7, 2010 and accepted July 5, 2010

DOI: 10.1021/am100312v

Published on Web 07/20/2010

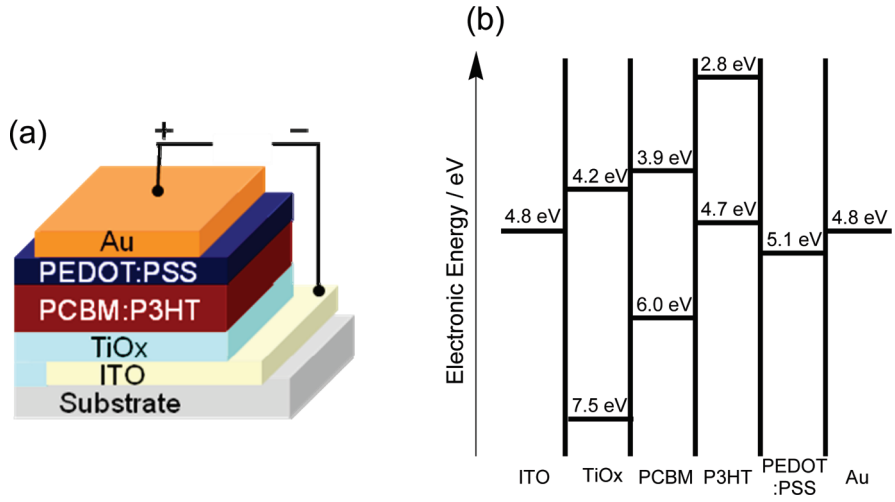

FIGURE 1. (a) Schematic diagram of the inverted organic solar cells. (b) Energy level diagram showing the work functions and the highest occupied and lowest unoccupied molecular orbital energies of the component materials.

the active layer is sandwiched between transparent indium tin oxide (ITO) and Al electrodes. In normal solar cells, the back Al electrode collects electrons because of its low work function. However, the performance of normal solar cells is quickly degraded when the Al electrode is not deposited under ultrahigh vacuum. Also, Al surfaces are easily oxidized to insulating Al_2O_3 by residual amounts of moisture and oxygen, so normal solar cells need to be completely sealed from the atmosphere. Therefore, to improve the durability of solar cells, it is crucially important to develop cells containing a noncorrosive electrode instead of Al. When an organic active layer is sandwiched between an ITO electrode and a noncorrosive Au electrode, photogenerated electrons flow from ITO to Au through an external circuit. These organic solar cells are called "inverted solar cells" because the electrons flow in the reverse direction to normal solar cells.

In our previous studies, we developed organic thin film solar cells using noncorrosive Au as the back electrode, and ITO/In, fluorine-doped tin oxide (FTO)/TiO_2 or TiO_x as the front electrode (13−15). For example, we found that a ITO/amorphous TiO_x/[6,6]-phenyl C_{61} butyric acid methyl ester (PCBM):regioregular poly(3-hexylthiophene) (P3HT)/poly(3,4-ethylenedioxylenethiophene):poly(4-styrene sulfonic acid) (PEDOT:PSS)/Au inverted solar cell showed a PCE of 2.47%. The performance of the sealed cell did not deteriorate after continuous light irradiation for 120 h in an ambient atmosphere (16). Even without sealing, this solar cell maintained its performance after continuous light irradiation for 20 h. Thus, we have the ability to fabricate organic thin-film solar cells exhibiting reasonable performance and stability. Many examples of organic thin film solar cells containing chemically stable n-type semiconductors TiO_2 (17, 18), ZnS (19), or ZnO (20−22) as an electron collection layer have been reported. We recently investigated inverted solar cells containing a ZnS (19) or ZnO (23) layer as an electron collection electrode by IS. However, the electrical properties of inverted solar cells are not yet sufficiently understood. In this paper, we report the complicated photoelectric properties and IS analysis of inverted organic bulk-heterojunction solar cells containing an amorphous TiO_x layer for electron collection (TiO_x cell).

2. EXPERIMENTAL SECTION

TiO_x cells were fabricated by the procedure described in one of our previous papers (16). An ITO electrode was ultrasonicated in 2-propanol, cleaned in boiling 2-propanol, and then dried in air. Cell fabrication was carried out in a N_2 filled glovebox containing less than 1 ppm moisture and oxygen as follows. A sol−gel TiO_x precursor solution containing titanium(IV) isopropoxide and acetyl acetone as a complexing agent in 2-methoxyethanol was spin-coated on the ITO electrode at 2000 rpm. The film was then hydrolyzed in a sealed container with the relative humidity controlled at around 45%. The precursor film was heated at 150 °C for 30 min on a hot plate to remove the solvent and complexing agent. A solution of P3HT (25 g L^{-1}) and PCBM (20 g L^{-1}) in 2,6-dichlorotoluene: chloroform (1:1 v/v) was spin-coated onto the ITO/TiO_x substrate and then the sample was heated at 120 °C for 20 min on a hot plate. Dispersions of PEDOT:PSS in water were spin-coated onto the PCBM:P3HT layer with a moisture concentration of around 50 ppm in the glovebox. An Au back electrode was vacuum deposited on the PEDOT:PSS layer. Finally, the device was heated at 150 °C for 5 min and then at 70 °C for 30 min. The effective area of the solar cell was restricted to 1.0 cm^2 by depositing the Au electrode using a shadow mask. A schematic diagram of the TiO_x cell is shown in Figure 1a.

The *I*−*V* curves of the solar cells were measured by linear sweep voltammetry (LSV) at a scan rate of 5 V min^{-1} under AM 1.5G simulated sunlight with 100 mW cm^{-2} intensity. The light source was a SAN-EI Electric XES-502S solar simulator calibrated by an EKO MS-601 pyranometer. The durability of the solar cells was tested using an interval LSV measurement in combination with rest voltage measurements under continuous irradiation from the simulated sunlight. All of the dc electric measurements were performed using a Hokuto Denko HZ-5000 electrochemical analyzer. IS measurements were obtained using a Hewlett-Packard precision *LCR* meter (4284A) in the dark and under simulated sunlight irradiation. The frequency range was from 20 Hz to 1 MHz, and the magnitude of the alternating signal was 5 mV. The obtained data were fitted with Scribner Associates Z-VIEW software v3.1 using the appropriate equivalent circuits. Ionization potentials for P3HT, PCBM, PEDOT:PSS, ITO, and Au were estimated using a Riken Keiki model AC-2 spectrometer and the band gap energies of P3HT

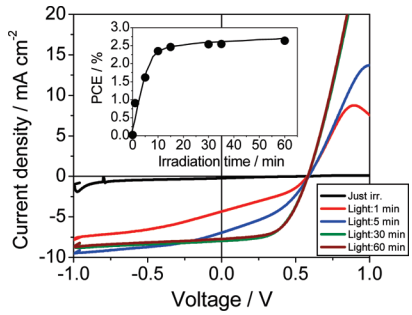

FIGURE 2. Time dependence of photo $I-V$ curve for the TiO_x cell. The inset shows a plot of PCE versus irradiation time for the TiO_x cell.

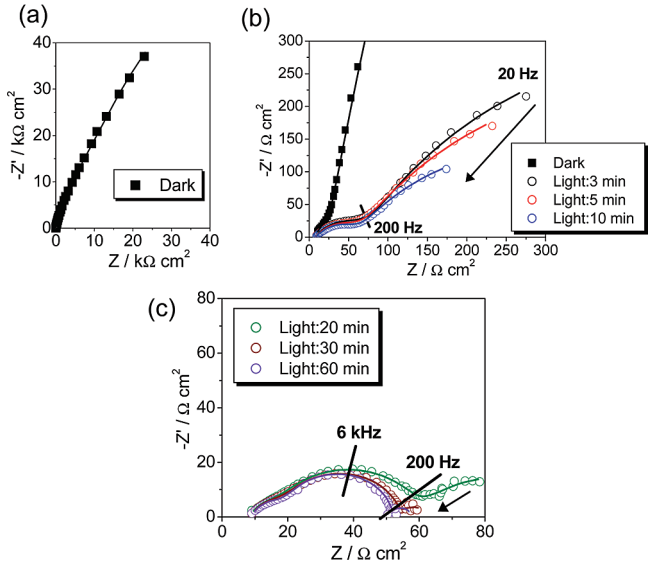

FIGURE 3. Typical Nyquist plots for the TiO_x cell at zero bias. Conditions: (a) dark; (b) under light irradiation for 3, 5, and 10 min; and (c) under light irradiation for 20, 30, and 60 min. The solid lines indicate fitting curves calculated using an equivalent circuit.

and PCBM were determined using a Hitachi U-3310 spectrophotometer. An energy level diagram for the component materials in the TiO_x cell is shown in Figure 1b. All measurements were carried out in an ambient atmosphere, that is, between 15 and 30 °C and with a relative humidity of 40−60%.

3. RESULTS AND DISCUSSION

Photoelectric Conversion Characteristics of the TiO_x Cell. The time dependences of the photo $I-V$ curves and the PCE of the TiO_x cell are shown in Figure 2. Photovoltaic behavior was hardly observed just after light irradiation. Upon continued light irradiation to the TiO_x cell, the photocurrent gradually increased and the PCE reached 2.55% after 60 min, with a short-circuit photocurrent (J_{sc}) of 7.73 mA cm^{-2}, an open-circuit photovoltage (V_{oc}) of 0.58 V, and a fill factor (FF) of 0.57.

IS measurements were carried out to investigate in detail the change in the performance of the TiO_x cell. Figure 3 shows the Nyquist plots for the TiO_x cell at zero bias in the dark (a) and under irradiation (b, c). In Figure 3c, three semicircles were clearly observed; at a highest frequency of more than 80 kHz, at a middle frequency of 80 kHz to 200 Hz, and at a lowest frequency of less than 200 Hz, which are denoted as semicircles 1, 2, and 3, respectively. In our

Scheme 1. Typical Equivalent Circuits for Nyquist Plots Containing Two and Three Semicircles

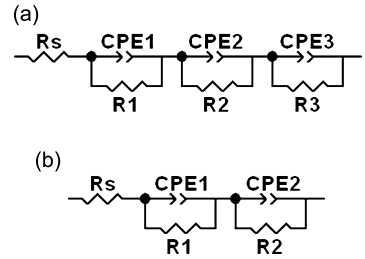

previous work (19, 23), Nyquist plots from the IS of FTO/ZnS/PCBM:P3HT/PEDOT:PSS/Au cells (ZnS cells) and FTO/ZnO/PCBM:P3HT/PEDOT:PSS/Au cells (ZnO cells) showed only two semicircles derived from the organic active layer and the n-type semiconductor layer. This indicates that the TiO_x cell has extra component to the ZnS and ZnO cells. The Nyquist plots in the dark and under irradiation were analyzed using an equivalent circuit as shown in Scheme 1a, which shows reasonable concordance with a simulated curve. Rs represents the series resistance consisting of ohmic components. R1, R2, and R3 are resistance components forming a parallel circuit with constant phase elements (CPE1, CPE2, and CPE3, respectively). The CPEs are roughly equal to differential capacitances because there was almost no depression of the semicircles. The Rs, R1, R2, and R3 values for the TiO_x cell in the dark were estimated to be 9, 11, 6.4×10^3, and 1.4×10^5 Ω cm^2, respectively, from the fitted curve. Though Rs and R1 for the TiO_x cell remained almost constant under irradiation, the R2 value gradually decreased from 6.4×10^3 Ω cm^2 in the dark to 32 Ω cm^2 after irradiation for 60 min. This large decrease in the resistance component is attributed to a large increase in the number of photoconductive carriers in the PCBM:P3HT film induced by light irradiation. This result indicates that the component in the middle-frequency range (semicircle 2) is derived from the organic active layer. The component in the highest-frequency range (semicircle 1) may be from TiO_x layer, from its analogy with the IS analysis of the ZnS and ZnO cells (19, 23). Unexpectedly, semicircle 3 almost completely disappeared after irradiation for 60 min. Only two semicircles, which were simulated by the equivalent circuit shown in Scheme 1b, were observed. Thus, IS analysis shows that the equivalent circuits of the TiO_x cells vary with irradiation time. That is, the plots in the dark and under light irradiation before disappearing semicircle 3 are simulated by the equivalent circuit shown in Scheme 1a, whereas the plots showing two semicircles under light irradiation are described very well by that in Scheme 1b. Figure 4 shows the time dependence of the R and PCE values of the TiO_x cell under light irradiation. R1 was virtually constant under irradiation for 60 min, whereas R2 and R3 decreased suddenly just after irradiation began and then very slowly, with the R3 component almost completely disappearing after 60 min. Thus the increase in PCE corresponded to the decrease of R2 and R3, so the photoresponsive characteristics of the TiO_x cell are mainly responsible for the presence of semicircle 3.

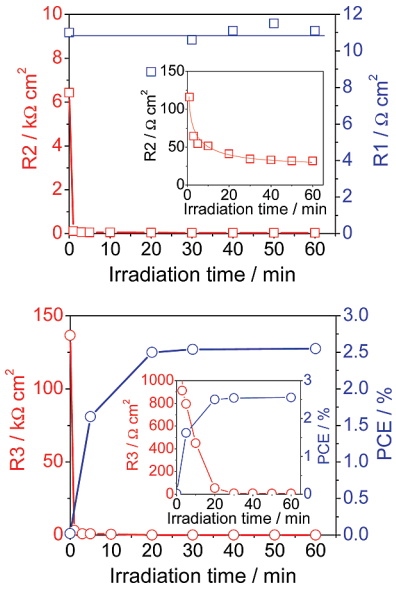

FIGURE 4. Time dependence of R and PCE values for the TiO_x cell under light irradiation. The insets show magnifications of the figures.

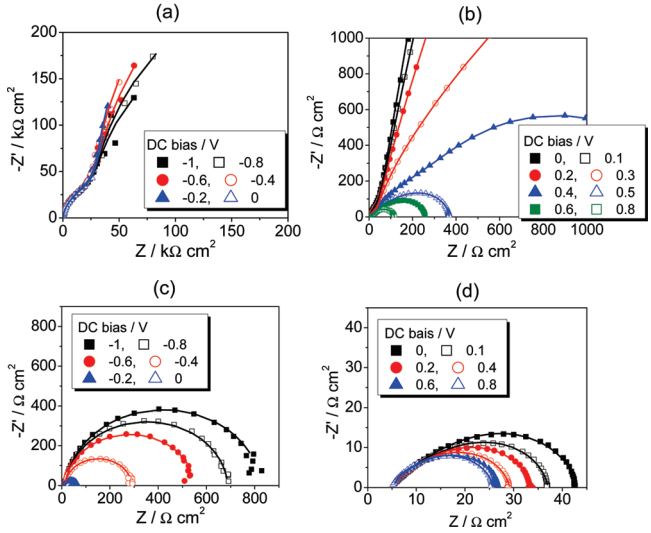

FIGURE 5. DC bias dependence of Nyquist plots for the TiO_x cell in the dark and under light irradiation. (a) In the dark, dc bias range; −1.0 to 0 V, (b) in the dark, dc bias range; 0 to +0.8 V, (c) under light, dc bias range; −1.0 to 0 V and (d) under light, dc bias range; 0 to +0.8 V. The solid lines indicate fitting curves calculated from equivalent circuits.

To analyze the ac impedance characteristics in more detail, a constant dc bias from −1.0 to +1.0 V was applied across the Au (positive) and ITO (negative) electrodes during the IS measurements. The TiO_x cell was irradiated with simulated sunlight for 60 min to obtain a stable cell performance before the IS measurement began. Figure 5 shows Nyquist plots of the TiO_x cell under a dc bias in the dark and under light irradiation. In the dark, the plots were almost unchanged by applying a reverse bias from −1.0 to 0 V (Figure 5a). In contrast, clear semicircles gradually appeared upon applying a forward bias from 0 to +1 V (Figure 5b). When a dc bias from −1.0 to +1.0 V was applied to the TiO_x cell under light irradiation, the semicircles diminished remarkably (Figure 5c,d).

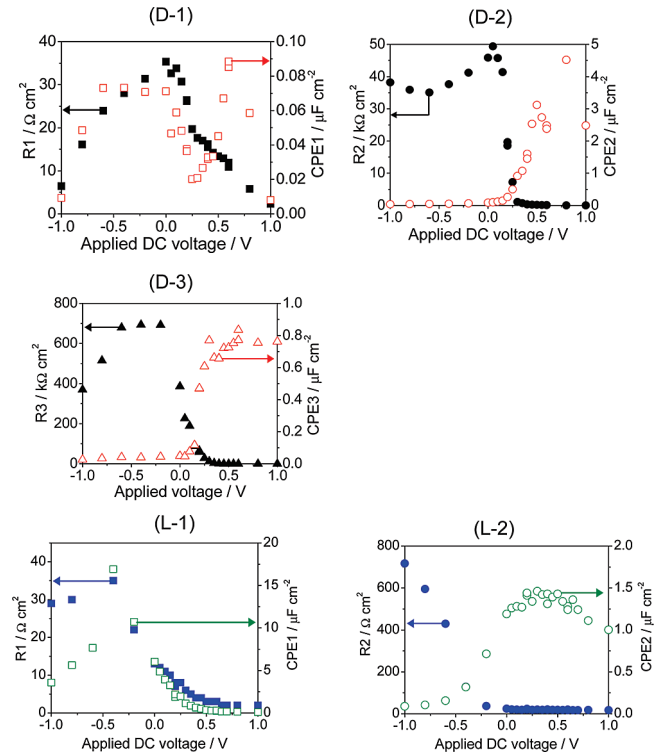

FIGURE 6. DC bias dependence of the R and CPE values for the TiO_x cell in the dark (D-1, D-2, and D-3) and under light irradiation (L-1 and L-2). D-1 and L-1 are plots of the higher-frequency component, D-2 and L-2 show the middle-frequency component, and D-3 is for the lower-frequency component.

Figure 6 shows the dc bias dependence of the R and CPE of the TiO_x cells in the dark and under light irradiation; these values were estimated from the simulated curves shown in Figure 5. When the dc bias decreased from +0.3 to 0 V in the dark, R2 suddenly increased as shown in Figure 6D-2. Simultaneously, CPE2 rapidly decreased when a dc bias of less than +0.6 V was applied. Because the dependences of R3 and CPE3 (Figure 6D-3) were almost the same as those of R2 and CPE2, the lowest-frequency component may originate from the PCBM:P3HT layer like the middle-frequency component. These results suggest that a depletion layer is formed on the PCBM:P3HT side of the TiO_x/PCBM:P3HT interface. Similar behavior was also observed for the high-frequency component shown in Figure 6D-1, although the very small CPE1 values were rather inconsistent. This indicates that a depletion layer is also formed on the TiO_x side of the TiO_x/PCBM:P3HT interface. The polarizability of these materials decreased because an electric field formed in the depletion layer forced TiO_x, PCBM, and P3HT molecules in the layers to polarize. As a result, the values of CPE1, CPE2, and CPE3 decreased, that is, the observed polarization capacities are limited by the internal electric field. On the other hand, the lowest-frequency component disappeared under light irradiation. The values of R2 and CPE2, which were estimated from the middle-frequency component, exhibited dc bias dependences similar to those in the dark (Figure 6L-2), although the dependence shifted significantly to a more negative value compared with that in the dark. These results shows that the electric fields in these depletion layers changed under light irradiation be-

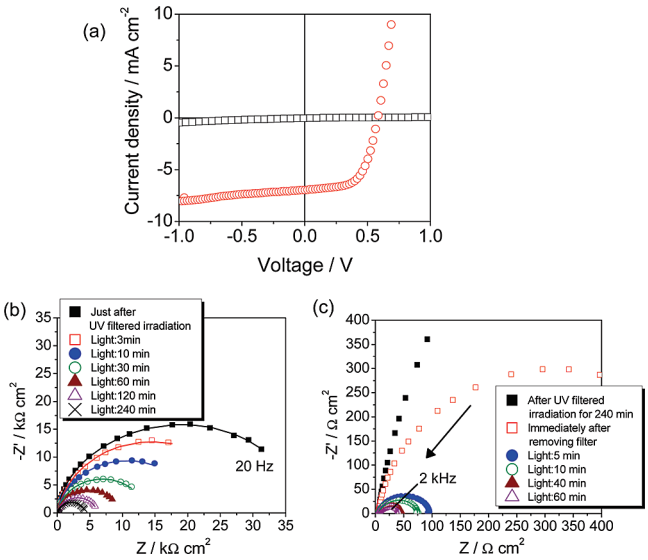

FIGURE 7. (a) Photo $I-V$ curves for the TiO_x cell under light irradiation with (black squares) and without a UV filter (red circles). Time dependence of Nyquist plots for the TiO_x cell at zero bias under light irradiation (b) with and (c) without a UV filter. The solid lines indicate fitting curves calculated from equivalent circuits. The data for c were obtained continuously after obtaining the data for b.

cause of the production of a large number of photo carriers in the PCBM:P3HT layer. The electric field profile for the TiO_x cell is almost the same as those for the ZnS and ZnO cells we reported previously (19, 23). However, the bias dependence of CPE1 as shown in Figure 6L-1, which was estimated from the highest-frequency component, cannot be fully explained at present.

To eliminate the influence of UV light of wavelength less than 440 nm in the simulated sunlight, a UV filter was used for the $I-V$ and IS measurements of the virgin TiO_x cell. A photocurrent was not completely observed upon irradiation with the filtered light (black squares in Figure 7a), although the semicircles obtained in the IS measurement decreased as the irradiation time increased, as shown in Figure 7b. To fit the Nyquist plots, the equivalent circuit shown in Scheme 1a is appropriate, even under irradiation with filtered light for over 4 h. As a result, Rs and R1 were almost constant under the filtered irradiation, but R2 and R3 gradually decreased from several tens-hundreds kΩ cm^2 in the dark to several kΩ cm^2. When the filter was subsequently removed, the photocurrent suddenly increased and at the same time semicircles 2 and 3 diminished (Figure 7c). This was followed by the disappearance of component 3 after 60 min, as well as the typical behavior shown in Figure 3. That is, irradiation with UV light was required to eliminate component 3. A maximum performance of PCE = 2.46% with J_{sc} = 6.96 mA cm^{-2}, V_{oc} = 0.58 V, and FF = 0.61 was obtained after irradiation for 60 min as shown by the red circles in Figure 7a. Furthermore, when the filter was subsequently reinserted, the PCE gradually decayed to 0.03% after 2 h (16). At the same time R3 appeared again and increased to about 300 Ω cm^2 (data not shown). It is known that holes accumulate on TiO_x surfaces upon irradiation with UV light. This may cause the PCBM molecules, in which the carbonyl oxygen atoms become partially negatively polarized, to move slightly in the photoactive layer toward the positive-charged TiO_x interface, forming an electron transporting pathway. That is, upon a morphological change in the photoactive organic layer, photogenerated electrons can be transported smoothly from the lowest unoccupied molecular orbital of the acceptor PCBM to the conduction band of TiO_x. However, when the UV filter was subsequently reinserted, the electron transporting pathway gradually disappeared, probably because holes slowly disappeared from the positively charged TiO_x interface and consequently the distance between the PCBM and the TiO_x increased.

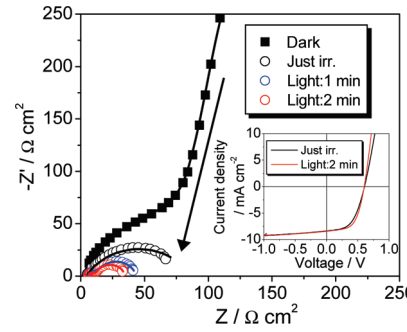

FIGURE 8. Time dependence of Nyquist plots for the surface-treated TiO_x cell under light irradiation at zero bias. The solid lines indicate fitting curves calculated from equivalent circuits. The inset shows photo $I-V$ curves for the surface-treated TiO_x cell immediately after beginning irradiation and after irradiation for 2 min.

Photoelectric Conversion Characteristics of a Surface-Treated TiO_x Cell. When TiO_x cells were fabricated in air except during spin-coating of the TiO_x film, it was noticed that the photovoltaic properties of the cells were remarkably influenced by environmental factors, especially the relative humidity. To investigate the influence of water on the cell performance, the TiO_x surface was made thoroughly wet by immersing the ITO/TiO_x electrode in distilled water, and then dried at 130 °C for 1 h. Figure 8 shows the time dependence of the Nyquist plots and the photo $I-V$ curves of such a surface-treated TiO_x cell. In this cell, a photocurrent was observed just after light irradiation, as shown by the black solid line in the inset. The maximum performance of PCE = 2.97% with J_{sc} = 8.46 mAcm^{-2}, V_{oc} = 0.60 V, and FF = 0.58 was obtained after 2 min of irradiation (red solid line in the inset). That is, the initial performance of the surface-treated TiO_x cell was considerably improved compared with that of the untreated cell. It is known that the cell performance can be altered by modifying the n-type semiconductor surface with various organic carboxylic acids, depending on the direction of the dipole and the magnitude of its moment at the n-type semiconductor/organic photoactive layer interface (21, 24–26). The enhanced photocurrent observed for the surface-treated TiO_x cell may be explained by the introduction of such a dipole. That is, strongly adsorbed water molecules still resided on the TiO_x surface even after drying the ITO/TiOx electrode at 130 °C for 1 h in air. The OH groups on the TiO_x surface became polarized to form $O^{\delta-}-H^{\delta+}$, where $\delta-$ and $\delta+$ represent partial charges in the OH group, because of hydrogen bonding with the adsorbed water molecules. This

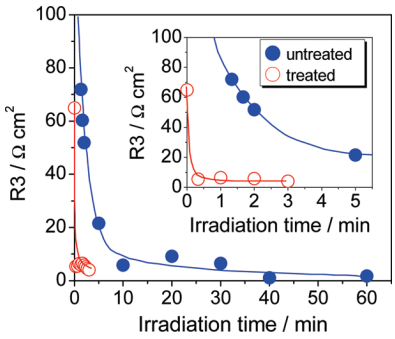

FIGURE 9. Time dependence of R3 for the untreated (blue circles) and surface-treated (red circles) TiO_x cells under light irradiation at zero bias. The inset highlights the initial 5 min of irradiation.

induces an increase in the electric field across the photo active organic layer, increasing the photocurrent by improving photogenerated charge separation.

According to the IS analysis of the surface-treated TiO_x cell, Rs and R1 were almost constant under irradiation, similar to those of the untreated cell. However, R2 decreased very quickly compared with the untreated cell. Furthermore, R3 decayed very rapidly and then disappeared unexpectedly (compare the red open circles for the surface-treated TiO_x cell with the blue solid circles for the untreated TiO_x cell in Figure 9), showing the time dependence of R3. The decay of R3 corresponded very well with the observed rapid increase of the PCE. The experimental results showed that a molecular contact that aided transportation of photogenerated electrons from PCBM to TiO_x was assisted by the water molecules adsorbed onto TiO_x. PCBM molecules may exist near the surface-treated TiO_x because weak hydrogen bonds could form between an adsorbed water molecule and the carbonyl oxygen of PCBM. When the TiO_x surface was positively charged by the accumulation of holes upon irradiation with UV light, partially polarized $\delta-$ carbonyl oxygen atoms in the PCBM molecules close to the TiO_x surface can be attracted quickly onto the TiO_x surface by relatively strong coulombic forces, smoothly transporting photogenerated electrons.

Although the surface-treated TiO_x cell exhibited excellent photoproperties initially, its durability in air was considerably inferior to that of the untreated TiO_x cell. The time dependence of $I-V$ curves of solar cells containing untreated and surface-treated TiO_x layers are shown in a and b in Figure 10, respectively. A comparison of the PCE against irradiation time for both cells is shown in Figure 10c. For the untreated cell, the PCE was almost maintained under continuous light irradiation for 10 h. In contrast, the PCE of the surface-treated cell decreased to ca. 80% of the maximum value after light irradiation for 10 h. This probably arises from a photocatalytic effect caused by the combination of titanium dioxide, water, and UV light. It is desired to realize the quick photoresponse and photocurrent enhancement achieved by the surface-treatment of TiO_x without the loss of durability that is found for surface treatment with water.

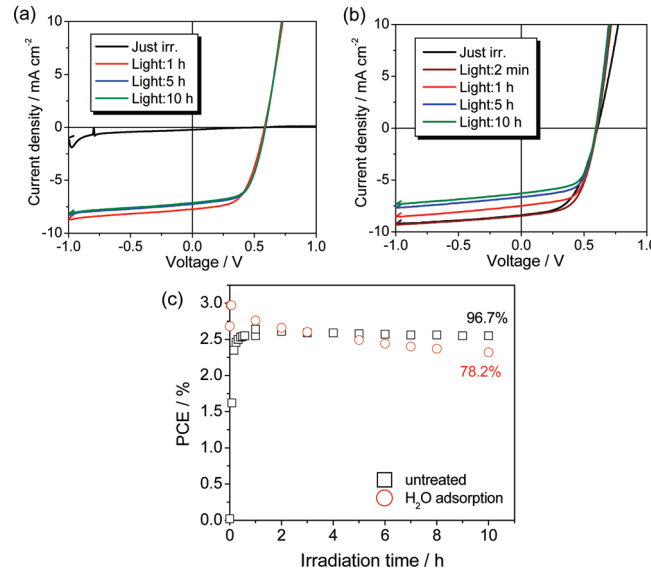

FIGURE 10. Irradiation time dependence of the photo $I-V$ curves for (a) the untreated TiO_x cell and (b) the surface-treated TiO_x cell under continuous irradiation in air. (c) Irradiation time dependence of the PCEs for the untreated TiO_x cell (blue squares) and the surface-treated TiO_x cell (red circles).

4. CONCLUSION

The photoelectric properties of inverted organic bulk-heterojunction solar cells containing amorphous TiO_x as an electron collection layer (TiO_x cell) were investigated by photo $I-V$ and IS measurements. The TiO_x cell exhibited an unusual characteristic of requiring a significant amount of time to reach its maximum PCE of 2.56%. The electrical resistance and capacitance for each layer in the solar cell was estimated using Nyquist plots to identify the origin of its slow photoresponse. Furthermore, to find the reason for this slow photoresponse in more detail, the influence of UV light present in the simulated sunlight was investigated, and a surface-treated TiO_x cell was fabricated using a TiO_x layer coated with adsorbed water molecules. A rapid photoresponse and enhanced performance (PCE = 2.97%) were observed for the surface-treated TiO_x cell, although its durability decreased considerably compared with that of the untreated cell. It was inferred from these experimental results that the slow photoresponse of the untreated TiO_x cell was because the morphology of the photoactive organic layer changed gradually, improving its ability to transport photocarriers at the TiO_x/PCBM:P3HT interface. This highlights the significance of designing electron collection layer/organic active layer interfaces exhibiting rapid electron transport to achieve highly efficient solar cells with a rapid photoresponse.

Acknowledgment. This work was supported by a Grant-in-Aid for Young Scientists (A) from the Ministry of Education, Culture, Sports, Science and Technology of Japan (21686011). This research was also supported by the "Global Environment Research Fund" from the Ministry of Environment, Japan (B-0807).

REFERENCES AND NOTES

(1) Kim, J. Y.; Lee, K.; Coates, N. E.; Moses, D.; Nguyen, T.-Q.; Dante, M.; Heeger, A. J. *Science* **2007**, *317*, 222.

(2) Liang, Y.; Wu, Y.; Feng, D.; Tsai, S.-T.; Son, H.-J.; Li, G.; Yu, L. *J. Am. Chem. Soc.* **2008**, *131*, 56.
(3) Hou, J.; Chen, H.-Y.; Zhang, S.; Chen, R. I.; Yang, Y.; Wu, Y.; Li, G. *J. Am. Chem. Soc.* **2009**, *131*, 15586.
(4) He, Y.; Chen, H.-Y.; Hou, J.; Li, Y. *J. Am. Chem. Soc.* **2010**, *132*, 1377.
(5) Han, L.; Koide, N.; Chiba, Y.; Mitate, T. *Appl. Phys. Lett.* **2004**, *84*, 2433.
(6) Wang, Q.; Moser, J.-E.; Gratzel, M. *J. Phys. Chem. B* **2005**, *109*, 14945.
(7) Li, Y.; Gao, J.; Yu, G.; Cao, Y.; Heeger, A. J. *Chem. Phys. Lett.* **1998**, *287*, 83.
(8) Jaiswal, M.; Menon, R. *Appl. Phys. Lett.* **2006**, *88*, 123504.
(9) Hsiao, C.-C.; Hsiao, A.-E.; Chen, S.-A. *Adv. Mater.* **2008**, *20*, 1982.
(10) Glatthaar, M.; Mingirulli, N.; Zimmermann, B.; Ziegler, T.; Kern, R.; Niggemann, M.; Hinsch, A.; Gombert, A. *Phys. Status Solidi A* **2005**, *202*, R125.
(11) Bisquert, J.; Garcia-Belmonte, G.; Antoni, M.; Sessolo, M.; Soriano, A.; Bolink, H. J. *Chem. Phys. Lett.* **2008**, *465*, 57.
(12) Garcia-Belmonte, G.; Antoni, M.; Barea, E. M.; Bisquert, J.; Ugarte, I.; Pacios, R. *Org. Electron.* **2008**, *9*, 847.
(13) Nakamura, J.-i.; Yokoe, C.; Murata, K.; Takahashi, K. *J. Appl. Phys.* **2004**, *96*, 6878.
(14) Takahashi, K.; Nishi, T.; Suzaka, S.; Sigeyama, Y.; Yamaguchi, T.; Nakamura, J.-i.; Murata, K. *Chem. Lett.* **2005**, *34*, 768.
(15) Takahashi, K.; Takano, Y.; Yamaguchi, T.; Nakamura, J.-i.; Yokoe, C.; Murata, K. *Synth. Met.* **2005**, *155*, 51.
(16) Kuwabara, T.; Nakayama, T.; Uozumi, K.; Yamaguchi, T.; Takahashi, K. *Sol. Energy Mater. Sol. Cells* **2008**, *92*, 1476.
(17) Kuwabara, T.; Sugiyama, H.; Yamaguchi, T.; Takahashi, K. *Thin Solid Films* **2009**, *517*, 3766.
(18) Mor, G. K.; Shankar, K.; Paulose, M.; Varghese, O. K.; Grimes, C. A. *Appl. Phys. Lett.* **2007**, *91*, 152111.
(19) Kuwabara, T.; Nakamoto, M.; Kawahara, Y.; Yamaguchi, T.; Takahashi, K. *J. Appl. Phys.* **2009**, *105*, 124513.
(20) Takanezawa, K.; Hirota, K.; Wei, Q.-S.; Tajima, K.; Hashimoto, K. *J. Phys. Chem. C* **2007**, *111*, 7218.
(21) Hau, S. K.; Yip, H.-L.; Ma, H.; Jen, A. K.-Y. *Appl. Phys. Lett.* **2008**, *93*, 233304.
(22) Hau, S. K.; Yip, H.-L.; Zou, J.; Jen, A. K.-Y. *Org. Electron.* **2009**, *10*, 1401.
(23) Kuwabara, T.; Kawahara, Y.; Yamaguchi, T.; Takahashi, K. *ACS Appl. Mater. Interfaces* **2009**, *1*, 2107.
(24) Khodabakhsh, S.; Sanderson, B. M.; Nelson, J.; Jones, T. S. *Adv. Funct. Mater.* **2006**, *16*, 95.
(25) Goh, C.; Scully, S. R.; McGehee, M. D. *J. Appl. Phys.* **2007**, *101*, 114503.
(26) Wei, Q.; Nishizawa, T.; Tajima, K.; Hashimoto, K. *Adv. Mater.* **2008**, *20*, 2211.

AM100312V